A force calibration standard for magnetic tweezers

Zhongbo Yu, David Dulin, Jelmer Cnossen, Mariana Köber, Maarten M. van Oene, Orkide Ordu, Bojk A. Berghuis, Toivo Hensgens, Jan Lipfert, and Nynke H. Dekker

---

Articles you may be interested in

Theoretical and experimental analysis of the forced LacI-AraC oscillator with a minimal gene regulatory model
Chaos **23**, 025109 (2013); 10.1063/1.4809786

High-force NdFeB-based magnetic tweezers device optimized for microrheology experiments
Rev. Sci. Instrum. **83**, 053905 (2012); 10.1063/1.4719916

Dual-trap optical tweezers with real-time force clamp control
Rev. Sci. Instrum. **82**, 083102 (2011); 10.1063/1.3615309

BaHigh-force magnetic tweezers with force feedback for biological applications
Rev. Sci. Instrum. **78**, 114301 (2007); 10.1063/1.2804771

Magnetically controlled gravity for protein crystal growth
Appl. Phys. Lett. **90**, 264105 (2007); 10.1063/1.2752718

A force calibration standard for magnetic tweezers

Zhongbo Yu, David Dulin,[a] Jelmer Cnossen, Mariana Köber, Maarten M. van Oene,
Orkide Ordu, Bojk A. Berghuis, Toivo Hensgens,[b] Jan Lipfert,[c] and Nynke H. Dekker[d]
Department of Bionanoscience, Kavli Institute of Nanoscience, Faculty of Applied Sciences, Delft University of Technology, Lorentzweg 1, 2628 CJ Delft, The Netherlands

To study the behavior of biological macromolecules and enzymatic reactions under force, advances in single-molecule force spectroscopy have proven instrumental. Magnetic tweezers form one of the most powerful of these techniques, due to their overall simplicity, non-invasive character, potential for high throughput measurements, and large force range. Drawbacks of magnetic tweezers, however, are that accurate determination of the applied forces can be challenging for short biomolecules at high forces and very time-consuming for long tethers at low forces below ∼1 piconewton. Here, we address these drawbacks by presenting a calibration standard for magnetic tweezers consisting of measured forces for four magnet configurations. Each such configuration is calibrated for two commonly employed commercially available magnetic microspheres. We calculate forces in both time and spectral domains by analyzing bead fluctuations. The resulting calibration curves, validated through the use of different algorithms that yield close agreement in their determination of the applied forces, span a range from 100 piconewtons down to tens of femtonewtons. These generalized force calibrations will serve as a convenient resource for magnetic tweezers users and diminish variations between different experimental configurations or laboratories. © *2014 AIP Publishing LLC.*
[http://dx.doi.org/10.1063/1.4904148]

INTRODUCTION

Advances in single-molecule instrumentation over the past two decades have resulted in high-resolution instruments capable of monitoring positions at the nanometer-scale with sub-second temporal resolution.[1–3] These developments make it possible to examine the biophysical properties of *in vitro* enzymatic reactions[4,5] and to develop accompanying theoretical models.[1] For example, it has become routine to monitor the progression of motor enzymes on a nucleic acid track at near-basepair resolution,[6,7] which makes it possible to unravel their underlying mechanochemistry.

Magnetic tweezers are a versatile single-molecule technique[1,8,9] that is capable of applying both forces and torques to tethered molecules. Magnetic tweezers can readily apply and measure forces in a wide range from >100 pN down to <10 femtonewtons (fN).[10] Compared to optical tweezers, magnetic tweezers are free from laser heating and photodamage. In addition, magnetic tweezers are simple to implement,[11] operate naturally in force clamp mode,[8] while still permitting direct switch to force ramp modes.[12] Furthermore, they are amenable to straightforward extensions that facilitate high throughput measurements,[3,13] torque measurements (using the magnetic torque tweezers[14–16]), twist measurements (using the freely orbiting magnetic tweezers[17]), or combinations thereof (e.g., using electromagnetic torque tweezers[18]).

There are two primary ways in which force calibrations can be performed in magnetic tweezers. The first is to compute the force from the gradient of the product between a bead's magnetization $(\vec{m}(\vec{B}))$ and the magnetic field $\vec{B}$ according to $\vec{F} = \frac{1}{2}\vec{\nabla}(\vec{m}(\vec{B}) \cdot \vec{B})$.[19,20] For a given type of superparamagnetic bead, however, the published magnetization values may differ from its true value[19] and, in addition, the accurate computation of magnetic fields can be challenging. Hence, a second approach relying on the sampling of a tethered magnetic bead's Brownian motion is commonly applied. From the variance of the transverse fluctuations together with the determination of the tether length (see below), the applied force can be deduced. This approach, too, comes with limitations. For example, using this Brownian motion approach, the duration of force measurement is inversely proportional to the applied force: particularly at the lowest applied forces, this measurement time can come to dominate the overall duration of the experiment. Additionally, particularly at high applied forces and/or with short tethers, one must take into account effects of the finite data acquisition frequency relative to the tethered bead's characteristic frequency to ensure accurate sampling of Brownian motion. Both of these limitations may be circumvented through the use of pre-determined force calibration curves, which would allow one to directly read off average force values for a given magnet position.

To provide detailed insight into the force calibration process for magnetic tweezers and facilitate standardization between different instruments from different laboratories, we

[a] Present address: Department of Physics, University of Oxford, Parks Road, Oxford OX1 3PU, United Kingdom.
[b] Present address: Department of Quantum Nanoscience, Kavli Institute of Nanoscience Delft, Delft University of Technology, Lorentzweg 1, 2628 CJ Delft, The Netherlands.
[c] Present address: Department of Physics, Nanosystems Initiative Munich, and Center for NanoScience, Ludwig-Maximilians-University Munich, Amalienstrasse 54, 80799 Munich, Germany.
[d] Author to whom correspondence should be addressed. Electronic mail: n.h.dekker@tudelft.nl

here present a complete set of calibration curves that covers the relevant force range for the vast majority of biological processes. We calibrate forces on two types of commonly used and commercially available superparamagnetic microspheres (or beads), MyOne and M270, for four alternative magnetic tweezers configurations that employ permanent magnets. The magnetic axes are aligned vertically above a flow cell with variable spacing between the two cubic magnets. Calibrations are carried out by coupling each bead to a glass surface via a double-stranded DNA (dsDNA) tethered to the bottom glass surface of a flow cell and measuring the Brownian motion.[21] A complete force calibration curve is constructed through successive measurements at different positions of the magnets above the flow cell. We calculate the resulting forces using four distinct algorithms and demonstrate that these are in excellent agreement with one another within the experimental limits for the acquisition frequencies. The force calibrations show excellent consistency between four different magnetic tweezers instruments. These generalized force calibrations, which span a range from 100 pN down to tens of fN, will serve as a convenient resource for any user setting up a magnetic tweezers instrument and diminish experimental variations between different experimental configurations or laboratories.

MATERIALS AND METHODS

Unless specified, chemicals are purchased from Sigma-Aldrich.

Magnetic tweezers instruments

A basic schematic of the magnetic tweezers is depicted in Figure 1.[19,22] Briefly, we use four different magnetic tweezers instruments that differ primarily in the types of objective and camera employed. Two of the instruments employ a $100\times$ magnification using an oil immersion objective (Numerical aperture (N.A.) = 1.25; UPLFLN $100\times$O2, Olympus, Tokyo, Japan) together with a CMOS camera (ac-
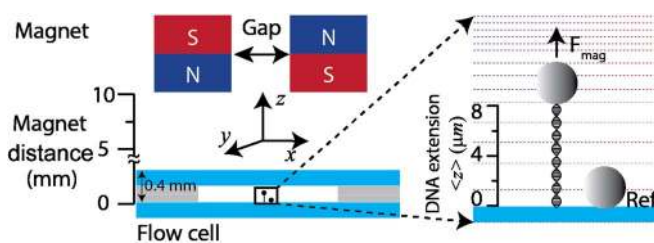

FIG. 1. Experimental scheme of the magnetic tweezers. The magnetic field in the magnetic tweezers is generated by a pair of vertically aligned magnets (S denotes the south pole (red) and N denotes the north pole (blue)). The gap between the two magnets has four sizes: 0.3, 0.5, 1, and 2 mm. The magnet distance is measured from the bottom surface of the flow cell to the bottom of the magnets, as indicated by the scale. The inset shows a DNA-tethered bead attached to the bottom surface of the flow cell, where $\langle z \rangle$ is the DNA extension measured from the bottom glass to the tethered bead. A reference bead (Ref) attached directly to the bottom surface of the flow cell is included to correct for drift in the instrument. Dotted color lines represent the magnetic field, where the field direction is indicated by the color transition from blue (north) to red (south). The force applied to the bead points in the direction of the gradient of the magnetic field. Cartesian coordinate directions are indicated, where x is the magnetic field direction and z is the gradient direction of the magnetic field.

quisition frequency 60 Hz; Dalsa Falcon 4M60, Ontario, Canada). The third employs a $60\times$ magnification using an oil immersion objective (N.A. = 1.25; UPLFLN $60\times$OI, Olympus) and a CCD camera (acquisition frequency 120 Hz; Pulnix TM-6710CL, CA, USA). The fourth employs a $200\times$ magnification using an oil immersion objective (N.A. = 1.49; CFI Apo TIRF $100\times$ Oil, Nikon, NY, USA) and a high speed CMOS camera (MC1362, Mikrotron, Germany) that is capable of acquiring frames at frequencies from 0.06 to 2 kHz. All four instruments employ an LED to illuminate the sample in the flow cell in transmission, a motorized stage (Physik Instrumente, M-126.PD, Karlsruhe, Germany) to control the vertical position of the magnets above the flow cell, and a rotary motor (Physik Instrumente, C-150) to control the magnets' rotation. Beneath each flow cell, a piezo-driven nanopositioning objective scanner (P-726.1CD, Physik Instrumente) controls the position of the inverted objective. The flow cell consists of a single channel formed by a shaped double-layer parafilm spacer sandwiched between two glass coverslips (Menzel-Gläser, 24×60 mm, #1, Braunschweig, Germany). The thickness of the parafilm spacer plus one glass coverslip is 0.4 mm, which is the inaccessible distance from the bottom of the magnets to the beads on the bottom surface inside the channel (Figure 1). The flow cell outlet connects to a peristaltic pump (ISM832C, Ismatec, Wertheim, Germany) for buffer exchange. A custom-written Labview 2011 program[23] is employed for data acquisition and device control. The focal shift axial scaling factor[24] that corrects for the refractive-index mismatch between oil and water, was set to 0.88 (the ratio of $n_{water}/n_{oil} = 1.33/1.51$).

Characteristic time scales of bead fluctuations

To accurately deduce forces via analysis of Brownian motion of a DNA-tethered bead in a harmonic trap, the characteristic timescale (τ) of the bead's motion sets boundaries for both the camera integration time (W) and the overall data collection time ($\tau_{measure}$). On the one hand, we need to sample this Brownian motion fast enough so that the $W < \tau$. On the other hand, $\tau_{measure}$ should be sufficiently longer than τ.[25] The characteristic timescale (or relaxation time, τ) under low Reynolds number conditions equals γ/k, where γ is the bead's friction coefficient and k the spring constant of the harmonic trap. In magnetic tweezers, k for motion in the transverse directions is given by the ratio between the force and DNA extension $\langle z \rangle$: $k = \frac{F}{\langle z \rangle}$.[26] Thus, the relaxation time may be expressed as $\tau = \frac{\gamma}{k} = \gamma\langle z \rangle/F$. Assuming γ is constant, the condition $W < \gamma\langle z \rangle/F < \tau_{measure}$ suggests that there are optimal experimental conditions of W, $\tau_{measure}$, and $\langle z \rangle$ for each force and tether length. For example, large values of $\langle z \rangle$ at a constant force allow for large values of W, which permits a slow acquisition frequency. In contrast, short values of $\langle z \rangle$ at a constant force reduce the duration of $\tau_{measure}$, and hence the overall measurement time. In this work, we use a 20.6 kbp DNA tether (corresponding to a contour length of 7.1 μm), a sufficiently long length to permit flexibility in the choice of cameras and their accompanying acquisition frequencies even

at high forces. In making this choice, we tolerate the lengthy values of $\tau_{measure}$ at low forces. Images are analyzed in real time at a specified acquisition frequency between 0.06 and 2 kHz.

The required time $\tau_{measure}$ for a desired accuracy can be estimated as:[27]

$$\tau_{measure} \approx \frac{12\pi^2 \eta R l_0}{F \varepsilon^2}, \qquad (F > 1\,pN)$$

or:

$$\tau_{measure} \approx \frac{8\pi^2 \eta R \xi l_0}{k_B T \varepsilon^2}, \qquad (F < 1\,pN),$$

where $\tau_{measure}$ is the minimum measurement time for a desired statistical accuracy ε (which we typically set to 0.05), η is the viscosity (0.001 Pa s for water), R is the bead radius, l_0 is the DNA contour length, F is the force at a particular magnet position, and ξ is the DNA persistence length[28] (equal to 47 nm under our experimental conditions of 10 mM Tris-HCl (pH = 7.4), 1 mM EDTA, and 100 mM NaCl).[29]

Magnet configurations and beads

Two 5 mm × 5 mm × 5 mm permanent magnets (Supermagnete, W-05-N50-G, Gottmadingen, Germany) are placed such that their magnetic moments are oriented vertically above the flow cell in anti-parallel directions (Figure 1). We employ four different gap sizes between these magnets (0.3 mm, 0.5 mm, 1 mm, and 2 mm). For each gap size, two types of superparamagnetic microspheres are employed for the calibrations, i.e., Dynabeads® MyOne (1 μm diameter, Cat# 65601, Invitrogen, Life Technologies, Carlsbad) and M270 beads (2.8 μm diameter, Cat# 65305, same manufacturer).

DNA construct and buffer conditions

We prepare a DNA construct as described in Ref. 26. In short, we use restriction enzymes of *Xho*I and *Not*I to digest a plasmid of Supercosl-lambda1,2, which results in two fragments.[26] We purify the fragment that is 20.6 kbp in length. The two ends of this purified DNA are ligated to biotin- and digoxigenin-functionalized polymerase chain reaction fragments (0.6 kb), respectively. All experiments are performed in a buffer containing 10 mM Tris-HCl (pH = 7.4), 1 mM EDTA, and 100 mM NaCl.

Assembly of the surface-DNA-bead system

We employ a similar procedure to assemble a flow cell for magnetic tweezers as previously reported.[26] First, we suspend 5 μl latex beads in ethanol (0.002% w/v, 3 μm diameter, Invitrogen, Life Technologies, Carlsbad) on a coverslip (Menzel-Gläser, Cat#: BB024060A1). Then, we heat the coverslip at 90 °C for 5 min to melt the beads onto the surface. A volume of 5 μl nitrocellulose (0.1% w/v in ethanol) is added to the coverslip to improve the adsorption of anti-digoxigenin antibodies in a subsequent step. After drying this coated coverslip at 90 °C for 5 min, we place a double-layer parafilm spacer containing a single channel on top. A second coverslip, pre-

drilled with two holes forming the inlet and outlet of the flow cell, is placed on top of this spacer. The resulting assembly is heated to melt the parafilm by pressing the flow cell against the hot plate at 90 °C for a few seconds, which provides a firm seal for the flow cell. We then functionalize the flow cell by flushing in 100 μl anti-digoxigenin antibodies (0.1 mg/ml in PBS, Roche) and incubating for 1 h. After washing with 1 ml of TE buffer with 100 mM NaCl, we load 100 μl of Bovine-Serum-Albumin containing buffer (1% BSA in 20 mM KPO$_4$, 50 mM NaCl, 0.1 mM EDTA, and 5% glycerol; New England Biolabs) into the flow cell, and incubate for 2 h.

Prior to tethering beads to the surface, we exchange the storage buffer of MyOne or M270 beads for TE buffer containing 100 mM NaCl. Next, we mix 1 μl DNA construct (0.8 ng/μl) with 9 μl washed MyOne or M270 beads (equivalent to 5 μl MyOne or 20 μl M270 beads at their stock concentrations, respectively). After incubation on ice for 10 min, we add 90 μl of TE buffer. Subsequently, 100 μl of DNA-bead mixture is flushed into the flow cell. Following a 10 min incubation period, we flush away beads that are not immobilized to the surface using the same buffer.

Once the DNA-tethered beads are attached in the flow cell, the application of the predominantly horizontally oriented magnetic field will orient them in the horizontal plane, a consequence of the beads' slight, but non-negligible magnetic anisotropy.[30] As a result, the attachment position of the DNA relative to the bottom of a bead will vary from bead to bead. Significant deviations from an attachment at the very bottom of the bead (Figure S1 in the supplementary material)[41] result in biased measurements of DNA extension,[31] $\langle z \rangle$. We selected beads that were attached near the bottom of the bead to limit the bias of the measured molecular extension to less than 5% (see Figure S1 in the supplementary material).[41]

RESULTS AND DISCUSSION

The forces applied to DNA-tethered magnetic beads in magnetic tweezers can be deduced by monitoring the Brownian motion of a bead about its equilibrium position.[21] By Taylor expanding the energy of the bead-DNA system to second order and using the equipartition theorem,[26] one can derive an expression for the applied force in terms of the DNA extension and the variance of the bead's Brownian motion:[9]

$$F = k_B T \langle z \rangle / \langle \delta x^2 \rangle, \qquad (1)$$

where k_B is the Boltzmann constant, T is the absolute temperature, $\langle z \rangle$ is the DNA extension, and $\langle \delta x^2 \rangle$ is the variance of the bead position. Repetition of such a measurement at various distances between the magnets and the magnetic beads then results in a complete calibration curve. In what follows, we make use of a 'magnet distance', which is defined such that the point where the bottom surface of the magnets would touch the lower inner surface of the flow cell is set to zero (Figure 1).

To illustrate such a measurement, we display a number of traces of bead motion (Figure 2(a)). These traces were acquired for an M270 bead tethered to a 20.6 kbp DNA and pulled upon by a pair of vertically aligned permanent magnets (Materials and Methods section). The gap size between the
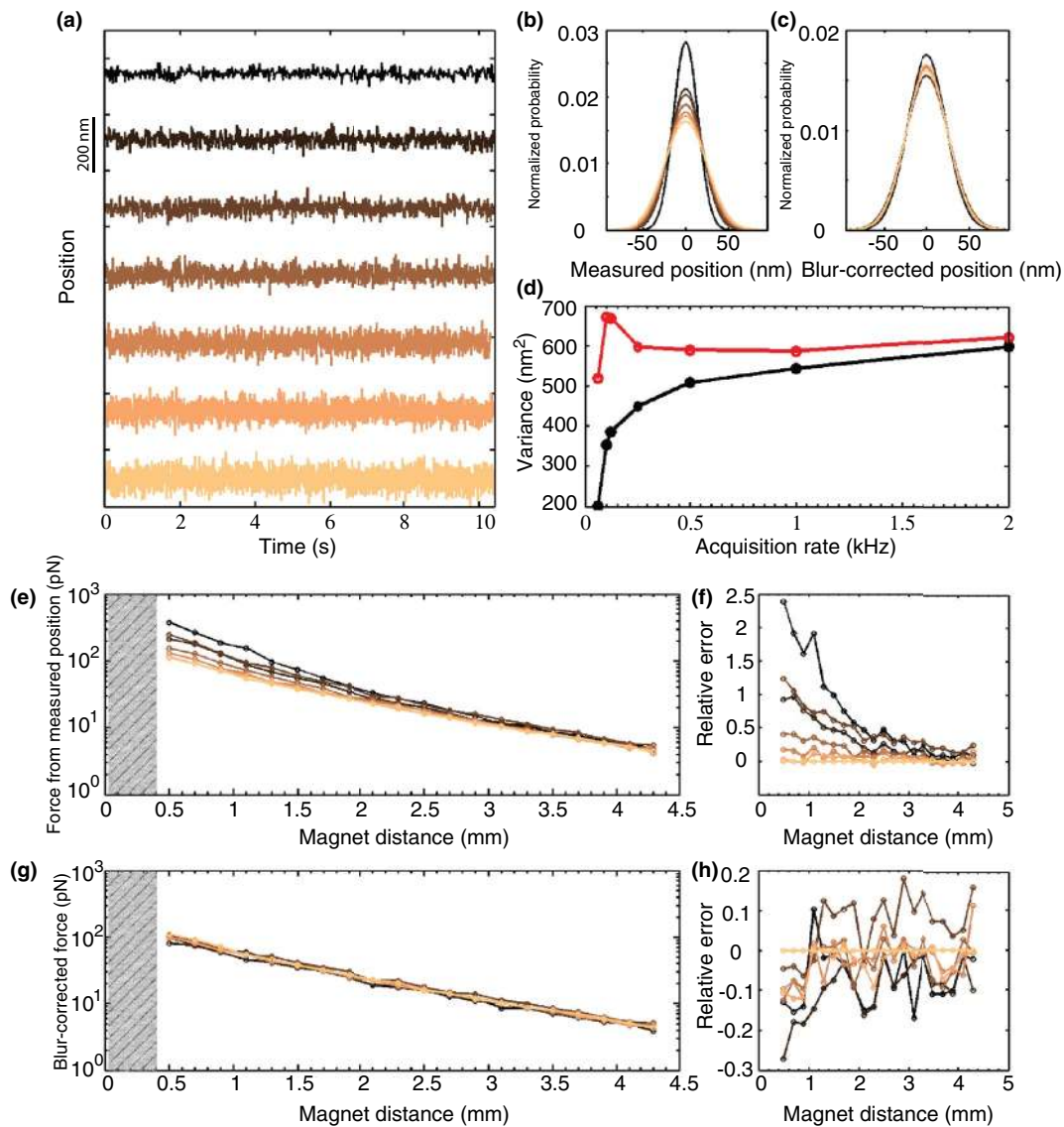
FIG. 2. Force calibration in the time domain. (a) The x positions of an M270 bead recorded at acquisition frequencies of 0.06, 0.1, 0.12, 0.25, 0.5, 1, and 2 kHz (dark to light colors) for a magnet gap size of 0.5 mm and a magnet distance of 1.1 mm for a duration of 10.5 s. Traces are collected from the same DNA-tethered bead, and offset upwards for clarity. (b) Histograms of the traces in (a). A blurring effect is visible: lower acquisition frequencies and longer integration times result in narrower histograms. (c) Histograms of the x positions of an M270 bead after the blur-correction[32] (details in main text). (d) Computed variances of the data in (b) before blur-correction (black) and of the corrected data in (c) (red). (e) Forces derived from the position variances as a function of magnet distance. Shaded area is inaccessible. (f) The errors in the forces in (e) relative to force values deduced directly from data obtained at 2 kHz. (g) Forces after the blur-correction. The shaded area is inaccessible due to the finite thickness of the flow cell. (h) The errors in the forces in (g) relative to that of data acquired at 2 kHz. The color code is the same in all panels apart from (d).

magnets equaled 0.5 mm, and the magnet distance was set to 1.1 mm. In principle, it would suffice to deduce the force from the variance of the transverse fluctuations (together with a measurement of the DNA extension $\langle z \rangle$). However, finite acquisition frequencies (f_s) bias the measured variance of the fluctuation and, therefore, affect the force measurement of magnetic tweezers, due to the time-averaging of the fluctuations over the finite integration time (W). The bias due to the finite acquisition time is particularly relevant when W is longer than the characteristic timescale (τ) of the bead's motion.[32] We here examine the effect of finite acquisition frequencies by collecting traces at the acquisition frequencies of 0.06, 0.1, 0.12, 0.25, 0.5, 1, and 2 kHz, respectively, where corresponding camera W equals to $W = 1/(2\pi f_s)$. In other

words, the camera shutter was continuously open (zero dead time) during the acquisition of an individual frame. The position histograms of traces recorded at different acquisition frequencies (Figure 2(b)) clearly demonstrate that longer shutter times result in reduced variances (quantified in Figure 2(d), black curve), and hence that simple computation of the variance does not provide a correct value for the applied force.

These differences in measured variances are clearly undesirable, as they result in systematic errors in the measured forces. Fortunately, the bias due to finite acquisition times can be corrected, as illustrated by Wong and Halvorsen[32] who introduced a motion blur correction function:

$$S(\alpha) = \frac{2}{\alpha} - \frac{2}{\alpha^2}\left(1 - \exp(-\alpha)\right), \qquad (2)$$

where α is the ratio of the camera integration time W to the characteristic timescale τ of a bead in a harmonic trap: $\alpha \equiv W/\tau$. Using the motion blur correction function, one can correct the measured variance $var(X_m)$ to obtain the true variance $var(X)$:

$$var(X) = \frac{var(X_m)}{S(\alpha)}. \qquad (3)$$

This permits the correction of underestimates that result from the use of $var(X_m)$. Such underestimates are particularly significant at high integration times (e.g., 74% of $var(X)$ for camera integration time $W = \tau$) and decrease for shorter integration times (e.g., 90% and 96.8% of $var(X)$ for $W = 1/3\tau$, $1/10\tau$, respectively). These computations indicate that, for the DNA tether length employed here, the use of the highest acquisition frequency (2 kHz) results in an accuracy of the force measurement by direct computation of the measured variance $var(X_m)$ that exceeds 90%. For reduced acquisition frequencies below 2 kHz, the use of Eq. (3) becomes imperative, and we can clearly observe the effect of the corrections on the histograms of bead positions (Figure 2(c)). The resulting values of $var(X)$ plotted as a function of the camera acquisition frequency (Figure 2(d), red curve) are in good agreement with the direct computation of the variance from data acquired at 2 kHz.

We plot the forces based on both the measured and corrected variances as a function of magnet distance (Figures 2(e)–2(g)). As expected, data acquired at low acquisition frequencies will result in overestimation of the true forces, with the relative errors being most pronounced in the high force regime where $\tau = \gamma/k$ is shortest (Figure 2(f)). For example, the relative error in the forces deduced from data acquired at 0.06 kHz (defined relative to forces deduced from data acquired at 2 kHz) increases from 0.2 to 2.5 as the magnets distance is decreased from 4.3 mm to 0.5 mm (Figure 2(f)). After correction, the relative errors are reduced to less than 0.1, provided that the acquisition frequencies exceed a lower bound (0.25 kHz) over the full range of magnet distances between 0.5 and 4.4 mm (Figure 2(h)). This lower bound can be decreased to 0.1 kHz if the magnet distances always exceed 2.4 mm. In other words, one can deduce accurate force values (to within 10%) from the analysis of bead positions in the time domain provided that the acquisition frequency exceeds certain limiting frequencies linked to the magnet distances employed.

An alternative method to calibrate the forces in magnetic tweezers[33] from bead positions in the time domain was proposed by Lansdorp *et al.* and relies on the computation of the Allan variance (Materials and Methods section). The Allan variance measures the signal stability over a given timescale to directly determine the uncorrelated noise and the magnitude of any drift.[34] In the Allan variance algorithm, one first averages the bead position over a certain sampling time. The difference between two consecutive samples of bead position is used to derive the ensemble-averaged variance, which is twice the Allan variance. Using the same data sets as above, we have computed the forces versus magnet positions according to this method (Figure S2 in the supplemen-

tary material).[41] The resulting forces display identical lower bounds on the acquisition frequencies as those deduced by employing the correction method introduced by Wong and Halvorsen.[32]

We note that the two preceding approaches to force calibration impose a lower bound on the acquisition frequency because we have fixed the camera exposure time at the inverse of the acquisition frequency. That is, the camera shutter is continuously open (zero dead time) and data are continuously averaged over this period. An alternative approach is to employ a lower camera speed with a reduced exposure time (non-zero dead time): for instance, one may acquire images at an acquisition frequency of 0.1 kHz and an exposure time of 1 ms (corresponding to 9 ms of dead time). Using such conditions, we have again measured forces, now on M270 beads tethered to the DNA pulled on by a pair of vertically aligned magnets separated by a gap size of 1 mm. Forces are computed from the variances of the bead positions in the time domain (Figure S3 in the supplementary material).[41] Within experimental error, the resulting forces agree with those deduced from data acquired at 2 kHz under zero dead time conditions. In other words, provided that enough light remains for illumination, the blurring effect can be significantly suppressed through the imposition of a non-zero dead time on a low speed camera. However, a drawback of this approach is that it results, for the same number of frames acquired, in an increased acquisition time compared to the strategy of employing zero dead time.

In addition to these approaches for correcting video-image motion blur from data in the time domain, there are two approaches operating in the frequency domain that can be used to determine the applied forces in magnetic tweezers.[21,33] As before, one starts by recording a bead's Brownian fluctuations, under conditions of zero camera dead time. One then makes use of the fact that bead motion in any dimension (the x dimension is selected here) in a medium with viscosity η can be described by a Langevin equation:[33]

$$kx + \gamma\dot{x} = F_L, \qquad (4)$$

where k is the spring constant of the harmonic system, γ is the drag coefficient equal to $6\pi\eta r$, and F_L is the Langevin force which obeys the fluctuation-dissipation relation: $\langle F_L(t + t_0)F_L(t)\rangle = 2\gamma k_B T\delta(t_0)$. We ignore the inertial force in the Eq. (4) because the friction occurs over an undetectable time interval, $\sim 10^{-6}$ s. Taking the magnitude of Fourier transform of this Langevin equation, one obtains the power spectral density (PSD) of bead motion as a function of frequency:[33]

$$P(f) = \frac{k_B T}{2\pi^2\gamma\left(f_c^2 + f^2\right)}, \qquad (5)$$

where f_c is a cut-off frequency equal to $k/2\pi\gamma$. We use two-sided power spectra throughout, so that integrating $P(f)$ over the range $(-\infty, +\infty)$ yields $\langle x^2\rangle = k_B T/k$. PSDs for the same dataset as in Figure 2(a) are plotted in Figure 3(a). As expected, the PSDs for datasets acquired at higher acquisition frequencies extend out to higher frequencies (compare the dataset acquired at 2 kHz to the datasets acquired at 1, 0.5, 0.25, 0.12, 0.1, and 0.06 kHz, Figure 3(a)), as do the corresponding fits to Lorentzian functions (shown in red). The data comprising such a PSD are, as before, subject to the
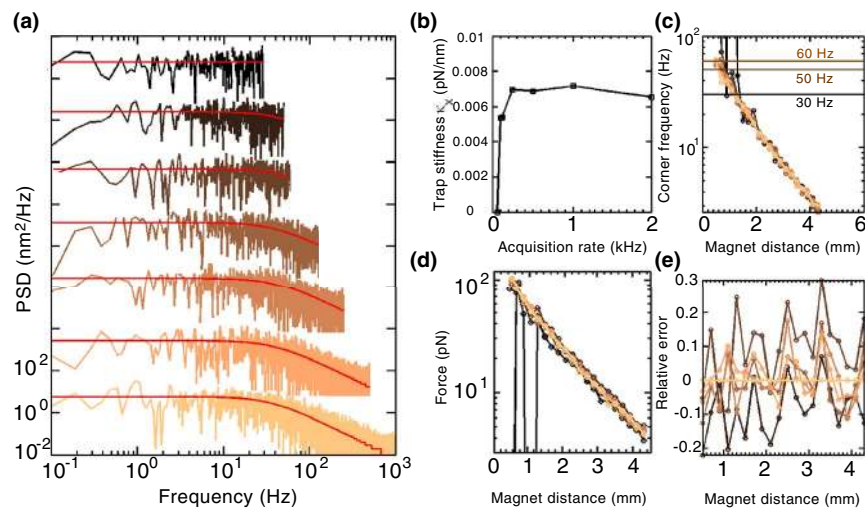
FIG. 3. Force calibration in the spectral domain. (a) Power spectra converted from the *x* positions in Figure 2(a) (identical color code) over the time interval of 10.5 s. The range of the spectra in the high frequency domain is limited by the acquisition frequencies employed. Fits of the spectra to Lorentzian functions are shown in red. Traces are offset upwards for clarity. (b) Trap stiffness versus acquisition frequency as deduced from the fits in (a). (c) Corner frequencies deduced from data acquired at different acquisition frequencies plotted as a function of magnet distance. Horizontal lines represent the Nyquist frequencies of 30, 50, and 60 Hz. (d) Forces derived from the PSD method described by te Velthuis *et al.*[21] as a function of magnet distance. The forces deduced at the acquisition frequency of 0.06 kHz show large fluctuations at low magnet distances. (e) The errors in the forces in (d) with respect to data obtained at 2 kHz. The results from data acquired at 0.06 kHz are not shown for clarity. The color code is the same in all panels apart from (b). The results above are deduced from the same DNA-tethered bead.

distorting effects of low-pass filtering and aliasing,[21,33] resulting in a biased measurement, $\tilde{P}(f)$. Previously, te Velthuis *et al.* have discussed[21] how to recover the underlying true PSD by fitting the integral of the power spectrum with an iterative and approximate correction. Using such an approach (denoted "te Velthuis PSD" in what follows) on data acquired for an M270 bead tethered to the DNA and pulled on by magnets at a distance of 1.1 mm, the computed trap stiffness (k_x) remains relatively constant for camera acquisition frequencies f_s exceeding 0.25 kHz (Figure 3(b)). Alternatively, for a camera acquisition frequency fixed at 0.1 kHz, the cut-off frequency that can be extracted from the datasets increases exponentially with magnet distance until $f_c > 40$ Hz (Figure S4 in the supplementary material).[41] When the magnet distance <1.4 mm (<0.7 mm) at the acquisition frequency of 0.06 kHz (0.1 kHz), proper determination of f_c is hampered by the limitations imposed by the Nyquist frequency (Figure 3(c)). The forces as a function of magnet distance that can be ex-

tracted from the datasets using this approach are shown in Figure 3(d). We observe that the forces derived using the te Velthuis PSD method deviate by less than 10% from to forces deduced from data acquired at 2 kHz, again provided that the camera acquisition frequency f_s exceeds a lower bound of 0.25 kHz over the range of magnet distances between 0.5 and 4.4 mm. This lower bound can be decreased to 0.1 kHz provided the magnet distances exceed 2.4 mm, in agreement with the result of computations in the time domain. A similar PSD-based approach has been detailed by Lansdorp *et al.* (denoted "Lansdorp PSD")[33] using an exact analytical expression to fit the PSD which is not based on the integral and thus more sensitive to drift. Using the same data sets as in Figure 2(a), we have also computed the forces using this approach (Figure S5 in the supplementary material),[41] which yields very comparable results.

The results of M270 beads pulled upon by a magnet configuration with a gap size of 0.5 mm can be summarized
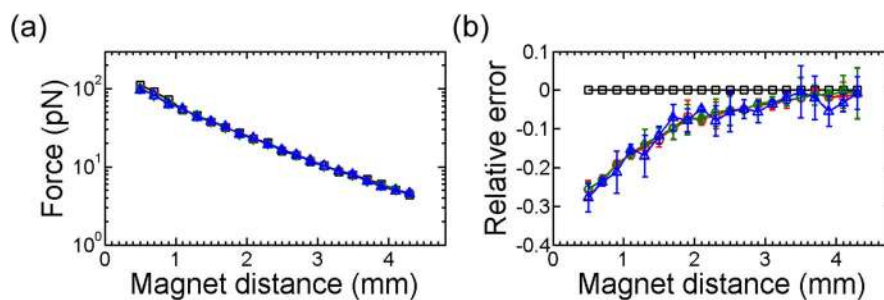

FIG. 4. Comparison of forces from four algorithms. (a) Forces on M270 beads as a function of magnet distance for a magnet gap size of 0.5 mm. The forces are derived from four algorithms: the estimate of the true variance from real-time data using the correction factor introduced by Wong[32] (black squares), the Allan variance method (green diamonds), the PSD method described by Lansdorp[33] (red circles), and the PSD method described by te Velthuis[21] (blue triangles). (b) Force deviations of the Allan variance and two PSD methods relative to that calculated by the variance with Wong's correction in real-time space.[32] Lines share the same color code as in (a). The results above are deduced on 5 measurements on the same DNA-tethered bead. Error bars represent the standard deviation.

in a plot that displays the forces that result from the four algorithms (Wong's motion blur correction function, Allan variance, te Velthuis PSD and Lansdorp PSD) for different magnet positions (Figure 4(a)). Data have been plotted for $f_s > 0.25$ kHz. From the overlap between the datasets, we can conclude that the algorithms generally provide very similar results. However, the high forces (typically corresponding to short magnet distances) diverge into two groups depending on the algorithm employed. Forces computed using the Allan variance approach or one of the two PSD-based methods lie below those deduced from the ones using Wong's motion blur correction function for magnet distances between 0.5 mm and 1.7 mm. Indeed, the relative errors between these approaches exceed 10% when the magnet distance is reduced below 1.7 mm (Figure 4(b)). The largest relative difference computed, 28%, is observed at a magnet distance of 0.5 mm, where $f_c = 62$ Hz. Since $W < 0.16\tau$ under our experimental conditions, the reliability of the forces deduced using Wong's motion blur correction function should exceed 95% (Eqs. (2) and (3)). This suggests that the other three algorithms underestimate the forces in this regime, as result of the fact that the cutoff frequency approaches the Nyquist frequency at low acquisition frequencies. We have shown previously that the spectral corrections for blurring and aliasing allow one to retrieve the correct forces within 10% error provided that the cutoff frequency does not exceed 80% of the Nyquist frequency.[21]

Thus far, we have employed four algorithms to calibrate the forces on M270 beads tethered by the DNA and pulled upon by a pair of vertically aligned magnets separated by a gap size of 0.5 mm over the range of magnet distances from 0.5 to 4.4 mm. We have applied different acquisition frequencies ranging from 0.06 to 2 kHz. Based on these measurements and their analysis, we can make recommendations for the best approaches to use. For magnet distances less than 2.4 mm (corresponding to forces > 16 pN), the best approach is to acquire data at high acquisition frequencies (e.g., 2 kHz), since no further data correction is required. If such a camera is not available, we recommend the use of Wong's motion blur correction function on data in the temporal domain. For magnet distances larger than 2.4 mm (corresponding to forces < 16 pN), more choices are available. Acquiring data at high acquisition frequencies (e.g., 2 kHz) remains a good option, although the collection of extensive datasets in this regime may challenge either the control software or the computer hardware. In this distance limit, our results illustrate that the errors in camera acquisition at low frequencies coupled with long integration time can be reliably corrected, irrespective of the algorithm employed, provided that the camera acquisition frequency exceeds 0.1 kHz. Thus, given their simplicity, we recommend the PSD-based methods for force calibration at magnet distances exceeding 2.4 mm. Matlab-based implementations of all these force calibration codes are available.[41]

To illustrate the use of these distinct approaches (analysis in either the time domain or the spectral domain), we calibrate forces on M270 beads over the full range of magnet distances between 0.5 and 10.4 mm. We choose to assemble separately acquired data at high forces (corresponding to magnet distances between 0.5 and 4.4 mm; acquired at a camera acquisition frequency of 2 kHz and analyzed in the time domain) and low forces (corresponding to magnet distances between 2.4 and 10.4 mm; acquired at a camera
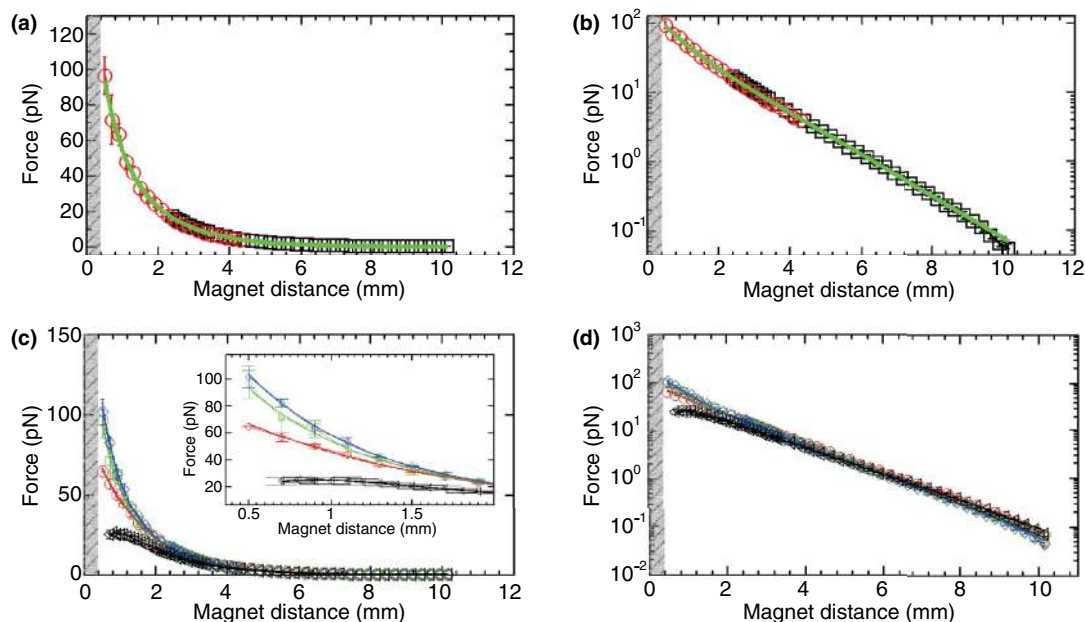

FIG. 5. Force calibration curves for M270 beads under four magnet gap sizes. (a) Force calibration curve assembled from two sections: the low force region in black squares (magnet distance from 2.4 to 10.4 mm, $N_{beads} > 10$) recorded at 0.10 kHz and the high force region in red circles (magnet distance from 0.5 to 4.4 mm, $N_{beads} > 5$) recorded at 2 kHz. The magnet gap size equals 0.5 mm. The green solid line represents the fit to a double exponential function. (b) Log-lin plot of the data in (a). (c) Force calibration curves of M270 beads ($N_{beads} > 5$) for four magnet gap sizes: 0.3 mm (blue diamonds), 0.5 mm (green squares), 1 mm (red circles), and 2 mm (black triangles). Solid lines represent the fit to a double exponential function. The inset zooms into the high force region. (d) Log-lin plot of the data in (c). Symbols represent the average of forces, and error bars indicate the standard deviations. The shaded area is inaccessible due to the finite thickness of the flow cell.

TABLE I. Double exponential fitting results from force-magnet distance curves. All forces were determined using the PSD method with correction of blurring and aliasing effects.[21] The units of force are in piconewtons. The units of the magnet distances and the gap sizes are in millimeters.

Index	Fit to a double exponential function	Magnet distance (mm)	Bead	Gap (mm)
1	$F(Z_{mag}) = -0.0078 + 43.5\exp(-(Z_{mag} - 0.4)/1.58) - 30.4\exp(-(Z_{mag} - 0.4)/0.319)$	0.7–10.4	M270	2
2	$F(Z_{mag}) = -2.74 + 71.8\exp(-(Z_{mag} - 0.4)/1.33) + 4\exp(-(Z_{mag} - 0.4)/36.9)$	0.5–10.4	M270	1
3	$F(Z_{mag}) = -0.0029 + 42.5\exp(-(Z_{mag} - 0.4)/0.49) + 62.8\exp(-(Z_{mag} - 0.4)/1.44)$	0.5–10.4	M270	0.5
4	$F(Z_{mag}) = -0.019 + 60.4\exp(-(Z_{mag} - 0.4)/0.563) + 56.9\exp(-(Z_{mag} - 0.4)/1.46)$	0.5–10.4	M270	0.3
5	$F(Z_{mag}) = -0.0028 + 5.69\exp(-(Z_{mag} - 0.4)/1.53) - 3.07\exp(-(Z_{mag} - 0.4)/0.351)$	0.5–10.4	MyOne	2
6	$F(Z_{mag}) = -0.117 + 8.68\exp(-(Z_{mag} - 0.4)/1.25) + 0.2\exp(-(Z_{mag} - 0.4)/14.5)$	0.5–10.4	MyOne	1
7	$F(Z_{mag}) = -0.0009 + 5.29\exp(-(Z_{mag} - 0.4)/0.52) + 7.16\exp(-(Z_{mag} - 0.4)/1.39)$	0.5–10.4	MyOne	0.5
8	$F(Z_{mag}) = -0.0009 + 6.21\exp(-(Z_{mag} - 0.4)/0.427) + 7.27\exp(-(Z_{mag} - 0.4)/1.35)$	0.5–10.4	MyOne	0.3

acquisition frequency of 0.1 kHz and analyzed in the spectral domain). The resulting force calibration curve for a magnet configuration with a gap size of 0.5 mm (Figure 5(a)) spans three orders of magnitude in force and shows excellent agreement in the overlapping region, i.e., magnet distances between 2.4 and 4.4 mm (log-lin plot of the same data shown in Figure 5(b)). Note that in this plot, the points correspond to the averages over several beads, with the error bars reflecting the corresponding standard deviations. For M270 beads, the variation between beads contributes to an uncertainty of 7%, which is within the range of error that is commonly accepted in force measurements.[17, 19, 35] This approach can be expanded to include magnet configurations with gap sizes of 2.0, 1.0, and 0.3 mm, which allows us to access an even larger range of forces (Figure 5(c); log-lin plots of the same data shown in Figure 5(d)). One can clearly note that the maximum force increases as the gap size between the magnets is reduced from 2 to 0.3 mm (Figure 5(c), inset). The maximum force measured equals ∼117 pN for magnets separated by a gap size of 0.3 mm and M270 beads. We additionally validate our force measurements using biological markers, e.g., the characteristic worm-like chain behavior of dsDNA[36] (Figure S6 in the supplementary material[41]). Additionally, B-form dsDNA undergoes a characteristic phase transition at an applied force of ∼65 pN[36–39] in which its extension increases by ∼70%. Using our force calibration curves, we find that this over-stretching transition occurs at 65 ± 5 pN in Tris-EDTA buffer (pH = 7.4) supplemented with 100 mM NaCl. In all cases, we fit the resulting force calibration curves as a function of magnet distance to a double exponential function:[40] $F(z) = \delta + \alpha_0 \exp(-z/\zeta_0) + \alpha_1 \exp(-z/\zeta_1)$, where z is the magnet position, F is the force, and δ, α_0, ζ_0, α_1, ζ_1 are fitting parameters. The resulting fits are summarized in Table I.

To enhance the generality of our calibration, we perform force measurements on MyOne beads using magnets separated by the same four gap sizes (0.3, 0.5, 1.0, and 2.0 mm). All other parameters are identical. Since MyOne beads have a lower magnetic moment than M270 beads, the characteristic frequency of their tethers ($f_c = \kappa/2\pi\gamma$) is reduced compared to that of M270-based tethers at the same magnet distance. Hence, an acquisition frequency of 0.1 kHz suffices to collect the full dataset. The resulting forces as a function of magnet distance display similar trends to those observed for the forces on M270 beads, with comparable uncertainty (8%) arising from bead-to-bead variations, but with much lower maximum applied forces, ∼14 pN (Figure S7 in the supplementary material).[41] The final fitting results of the double exponential functions are summarized in Table I.

Our laboratory has recently developed a novel bead tracking software package[23] (freely available at nynkedekkerlab.tudelft.nl) that employs a combination of Labview, C++ and CUDA to enable the parallel tracking of multiple beads (e.g., tracking 1000 beads at an acquisition frequency of 20 Hz) or high speed tracking of beads (e.g., tracking two beads at an acquisition frequency of 10 kHz) in magnetic tweezers. In this work, we have employed this software package to collect all datasets. Under the conditions of the DNA tethered M270 beads, a pair of vertically aligned magnets with 1 mm gap size, and an acquisition frequency of 2 kHz at high forces and 0.1 kHz at low forces, the resulting calibration curve agrees well with that obtained by the predecessor Labview package (Figure S8 in the supplementary material),[41] which has been used in a series of published works.[19, 21, 26] The present force calibration thus validates the newly developed package. In addition, we have cross-validated these force calibrations on four different magnetic tweezers instruments, which reveals excellent agreement (Figure S9 in the supplementary material).[41]

CONCLUSIONS

Magnetic tweezers have become a popular and robust technique to measure the forces applied to or generated by biological molecules. To provide detailed insight into the force measurement and facilitate standardization of the conventional permanent magnet-based magnetic tweezers, we have presented a complete set of calibrated look-up tables of the achievable forces on two different types of beads for four alternative magnet configurations. The achievable forces range from more than 110 pN down to 8 fN, while the force calibrations show excellent consistency on four independent magnetic tweezers instruments. We anticipate that the generalized force calibrations demonstrated here will not only serve as convenient look-up tables for any user but also help to limit experimental variations from instrument to instrument.

ACKNOWLEDGMENTS

[1] I. De Vlaminck and C. Dekker, Annu. Rev. Biophys. **41**, 453 (2012).
[2] K. C. Neuman and A. Nagy, Nat. Methods. **5**, 491 (2008).
[3] N. Ribeck and O. A. Saleh, Rev. Sci. Instrum. **79**, 094301 (2008).
[4] D. A. Koster, A. Crut, S. Shuman, M.-A. Bjornsti, and N. H. Dekker, Cell **142**, 519 (2010).
[5] D. Dulin, J. Lipfert, M. C. Moolman, and N. H. Dekker, Nat. Rev. Genet. **14**, 9 (2012).
[6] E. A. Abbondanzieri, W. J. Greenleaf, J. W. Shaevitz, R. Landick, and S. M. Block, Nature (London) **438**, 460 (2005).
[7] M. Manosas, A. Meglio, M. M. Spiering, F. Ding, S. J. Benkovic, F. X. Barre, O. A. Saleh, J. F. Allemand, D. Bensimon, and V. Croquette, Methods Enzymol. **475**, 297 (2010).
[8] D. A. Koster, V. Croquette, C. Dekker, S. Shuman, and N. H. Dekker, Nature (London) **434**, 671 (2005).
[9] T. R. Strick, J. F. Allemand, D. Bensimon, A. Bensimon, and V. Croquette, Science **271**, 1835 (1996).
[10] T. Strick, J.-F. Allemand, V. Croquette, and D. Bensimon, Prog. Biophys. Mol. Biol. **74**, 115 (2000).
[11] T. Lionnet, J. F. Allemand, A. Revyakin, T. R. Strick, O. A. Saleh, D. Bensimon, and V. Croquette, Cold Spring Harb Protoc. **2012**, 133 (2012).
[12] M. Kruithof, F. Chien, M. de Jager, and J. van Noort, Biophys. J. **94**, 2343 (2008).
[13] I. De Vlaminck, T. Henighan, M. T. van Loenhout, I. Pfeiffer, J. Huijts, J. W. Kerssemakers, A. J. Katan, A. van Langen-Suurling, E. van der Drift, C. Wyman, and C. Dekker, Nano Lett. **11**, 5489 (2011).
[14] J. Lipfert, J. W. Kerssemakers, T. Jager, and N. H. Dekker, Nat. Methods **7**, 977 (2010).
[15] F. Mosconi, J. F. Allemand, and V. Croquette, Rev. Sci. Instrum. **82**, 034302 (2011).
[16] A. Celedon, I. M. Nodelman, B. Wildt, R. Dewan, P. Searson, D. Wirtz, G. D. Bowman, and S. X. Sun, Nano Lett. **9**, 1720 (2009).
[17] J. Lipfert, M. Wiggin, J. W. Kerssemakers, F. Pedaci, and N. H. Dekker, Nat. Commun. **2**, 439 (2011).
[18] X. J. Janssen, J. Lipfert, T. Jager, R. Daudey, J. Beekman, and N. H. Dekker, Nano Lett. **12**, 3634 (2012).
[19] J. Lipfert, X. Hao, and N. H. Dekker, Biophys. J. **96**, 5040 (2009).
[20] K. C. Neuman, T. Lionnet, and J.-F. Allemand, Annu. Rev. Mater. Res. **37**, 33 (2007).
[21] A. J. te Velthuis, J. W. Kerssemakers, J. Lipfert, and N. H. Dekker, Biophys. J. **99**, 1292 (2010).
[22] J. Lipfert, J. J. Kerssemakers, M. Rojer, and N. H. Dekker, Rev. Sci. Instrum. **82**, 103707 (2011).
[23] J. P. Cnossen, D. Dulin, and N. H. Dekker, Rev. Sci. Instrum. **85**, 103712 (2014).
[24] M. T. van Loenhout, J. W. Kerssemakers, I. De Vlaminck, and C. Dekker, Biophys. J. **102**, 2362 (2012).
[25] C. Gosse and V. Croquette, Biophys. J. **82**, 3314 (2002).
[26] J. Lipfert, D. A. Koster, I. D. Vilfan, S. Hage, and N. H. Dekker, Methods Mol. Biol. **582**, 71 (2009).
[27] T. Strick, Ph.D. thesis, The University of Paris VI, 1999.
[28] C. G. Baumann, S. B. Smith, V. A. Bloomfield, and C. Bustamante, Proc. Natl. Acad. Sci. U.S.A. **94**, 6185 (1997).
[29] J. R. Wenner, M. C. Williams, I. Rouzina, and V. A. Bloomfield, Biophys. J. **82**, 3160 (2002).
[30] M. van Oene, L. Dickinson, F. Pedaci, M. Köber, D. Dulin, J. Kerssemakers, J. Lipfert, and N. H. Dekker, "The torque on superparamagnetic beads in magnetic fields" (unpublished).
[31] D. Klaue and R. Seidel, Phys. Rev. Lett. **102**, 028302 (2009).
[32] W. P. Wong and K. Halvorsen, Opt. Express **14**, 12517 (2006).
[33] B. M. Lansdorp and O. A. Saleh, Rev. Sci. Instrum. **83**, 025115 (2012).
[34] D. W. Allan, Proc. IEEE **54**, 221 (1966).
[35] I. De Vlaminck, T. Henighan, M. T. van Loenhout, D. R. Burnham, and C. Dekker, PLoS One **7**, e41432 (2012).
[36] C. Bouchiat, M. D. Wang, J. Allemand, T. Strick, S. M. Block, and V. Croquette, Biophys. J. **76**, 409 (1999).
[37] C. Bustamante, Z. Bryant, and S. B. Smith, Nature (London) **421**, 423 (2003).
[38] C. G. Baumann, V. A. Bloomfield, S. B. Smith, C. Bustamante, M. D. Wang, and S. M. Block, Biophys. J. **78**, 1965 (2000).
[39] M. D. Wang, H. Yin, R. Landick, J. Gelles, and S. M. Block, Biophys. J. **72**, 1335 (1997).
[40] H. Chen, H. Fu, X. Zhu, P. Cong, F. Nakamura, and J. Yan, Biophys. J. **100**, 517 (2011).
[41] See supplementary material at http://dx.doi.org/10.1063/1.4904148 for Figures S1-S9 and the Matlab codes used to compute forces from bead fluctuations. The latter information is also available at nynkedekkerlab. tudelft.nl.